



Weld quality characterization by vibration analysis for ultrasonic metal welding processes[☆]

Florian W. Müller^{a,1,*}, Christian Mirz^{b,2,*}, Sascha Weil^{b,*}, Alexander Schiebahn^{a,3}, Burkhard Corves^{b,4}, Uwe Reisgen^{a,5}

^a ISF RWTH Aachen University, Aachen, Germany

^b IGMR RWTH Aachen University, Aachen, Germany

ARTICLE INFO

Keywords:

Ultrasonic metal welding
Vibration analysis
Process monitoring
Vibration measurements
Random forest
Automated data processing
Machine learning

ABSTRACT

Ultrasonic metal welding is an efficient, solid-state welding process that is well established in the production of electrical equipment. However, isolated and untraceable failures occasionally occur in industrial production processes. According to the state of the art, these failures are due to a multitude of influencing variables, such as material and surface condition of the joining partners, as well as tool and fixture wear. This study presents quality prediction models based on measurements of mechanical vibrations of the welding machine using laser triangulation sensors, sonotrode penetration depth measurements, and machine internal welding power signals. The acquired data are processed and transformed into a random forest model to estimate the shear strength of the welds. The robustness of the prediction model has been successfully validated by welding experiments with significant external disturbances, such as surface roughness, contamination and material hardness. Within the framework of this study, the development of a stable and industrially applicable concept for process monitoring is demonstrated with a regression model that achieves a mean relative estimation error of 4.30% and a R^2 value of 0.964. Furthermore, a classification model that determines the external disturbances for the individual welds was successfully validated, achieving a micro $F1$ value of 94% and a macro $F1$ value of 95%.

Introduction

Modern vehicles, systems, and devices increasingly rely on electrified components and digital controls. This increase is driven by technology trends, such as electromobility and autonomous driving (Agency; Bansal and Kockelman, 2017). In these applications, the ability to reliably transport and store energy and information is essential for success. As a result, there is not only growing interest in, but also increasing demands on, suitable manufacturing processes. One example of such a manufacturing process is ultrasonic metal welding (USMW), which is used in the production of battery cells, high-power electronics and

wiring harnesses for modern automobiles. Ultrasonic metal welding is a solid-state welding process that is used primarily in demanding electrical and electronic applications, as it allows large joint cross sections and causes low heat input (Reisgen and Stein, 2016; Wodara and Adam, 2004). It is easy to automate, energy-efficient and allows the welding of dissimilar metals with limited intermetallic formation, as well as the joining of multiple layers of sheets and foils or wire strands in a single joining operation. The high joint quality precludes meaningful characterization of USMW joints by electrical properties, such as contact resistance Sievers, Völlner and Essers (21.11.2017). Instead, joint quality is quantified by destructive mechanical testing. Therefore,

* This research was funded by the German Federation of Industrial Research Associations (AiF) and continued by funds of the Deutsche Forschungsgemeinschaft (DFG - German Research Foundation) under Grant Number 520475171 "Hybrid Process Prognosis for Metal Ultrasonic Welding - Pro²MUSS".

[☆] Corresponding authors.

E-mail addresses: florian.mueller@isf.rwth-aachen.de (F.W. Müller), mirz@igmr.rwth-aachen.de (C. Mirz), sacha.weil@claimflow.de (S. Weil), schiebahn@isf.rwth-aachen.de (A. Schiebahn), corves@igmr.rwth-aachen.de (B. Corves), office@isf.rwth-aachen.de (U. Reisgen).

¹ ORCID: 0000-0001-7435-2357

² ORCID: 0000-0002-5270-9842

³ ORCID: 0000-0001-8427-6765

⁴ ORCID: 0000-0003-1824-3433

⁵ ORCID: 0000-0003-4920-2351

welding parameters for industrial applications and research are typically optimized for the mechanical properties of the joint (Bergmann et al., 2017; Elangovan et al., 2010; Heinz et al., 2012; Köhler et al., 2019; Pauleser et al., 2016; Poovannan, 2015; Satpathy et al., 2015). While USMW is standardized for certain applications (Reisgen and Stein, 2016; International, 05.04.2016; Wodara and Adam, 2004), the joint formation and the influences on the welding process are not yet fully understood (Balz, 2020). Furthermore, the welding process is prone to a large number of disturbances, which lead to fluctuating joint quality without apparent change in boundary conditions. Due to the large number of influencing variables with simultaneously increasing expectations on joint quality and process reliability, the development and validation of suitable monitoring methods is necessary.

Ultrasonic metal welding process and process influences

A simplified description of a USMW process can be as follows: Several workpieces (metal sheets, foil stacks, stranded wires, wire terminals) are placed on top of each other on the anvil. A sonotrode (also known as a horn) is then placed on top of the workpieces and exerts a vertical force on them. This force is counteracted by the anvil below. After reaching a predetermined process force, the sonotrode is excited into its working vibration perpendicular to the process force. Typically, the oscillation frequency is in the range of 20 kHz to 60 kHz and the amplitude is in the range of 10 µm to 50 µm. The oscillation causes relative motion between the sonotrode, the workpieces and the anvil, which causes friction, local heat generation and plastic deformation (Balz, 2020). This leads to the formation and growth of micro-welds in the joining area, as well as changes in the microstructure (Adam et al., 2004; Balz, 2020; Wodara and Adam, 2004).

In practical applications, the oscillation is exerted by reed sonotrode, linear sonotrode (λ -half and λ designs, referring to the standing wave in the tool), torsional sonotrode and similar Wodara and Adam (2004). The sonotrode design is decided based on, among other considerations, the accessibility of the weld area and the geometry and size of the required

joint. The anvil geometries and additional fixtures, such as clamping and alignment devices are also adapted to the workpieces and joint type. Figure 2 shows a linear oscillation system consisting of a horn, a booster, a transducer and the generator. The Figure also includes the vertical process force F described previously and the lateral standing wave (red line) characterizing the sonotrode oscillations. The oscillation is defined by the generator, which produces a high-voltage alternating current. This oscillation is converted into a mechanical oscillation in the transducer; modern transducers accomplish this by using stacked piezoelectric ceramic elements. The booster serves as a mechanical support for the oscillation system. Furthermore, it stabilizes the oscillation and, if necessary, is used to amplify its amplitude according to a factor determined by its shape. Finally, the sonotrode transforms the mechanical oscillation of the booster to the working amplitude and transmits it to the workpieces. All oscillating parts are tuned to match the working frequency of the particular machine, e.g. a machine designed for a working frequency of 20 kHz machine requires tools with a natural frequency close to 20 kHz. The anvil is usually rigid and holds the lower workpiece in place. Figure 2 shows the knurled surface of the horn and

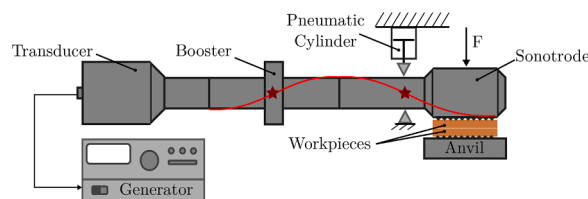


Fig. 2. The figure shows the setup for the welding experiments presented later. The variable F represents the vertical process force F exerted by the sonotrode on the workpieces, perpendicular to its direction of oscillation. This force is generated by a pneumatic cylinder. The lateral standing waveform, which characterizes the sonotrode oscillations, is indicated by a red line. The knots of the waveform, which represent points where the vibration amplitude is zero, are indicated by red stars.

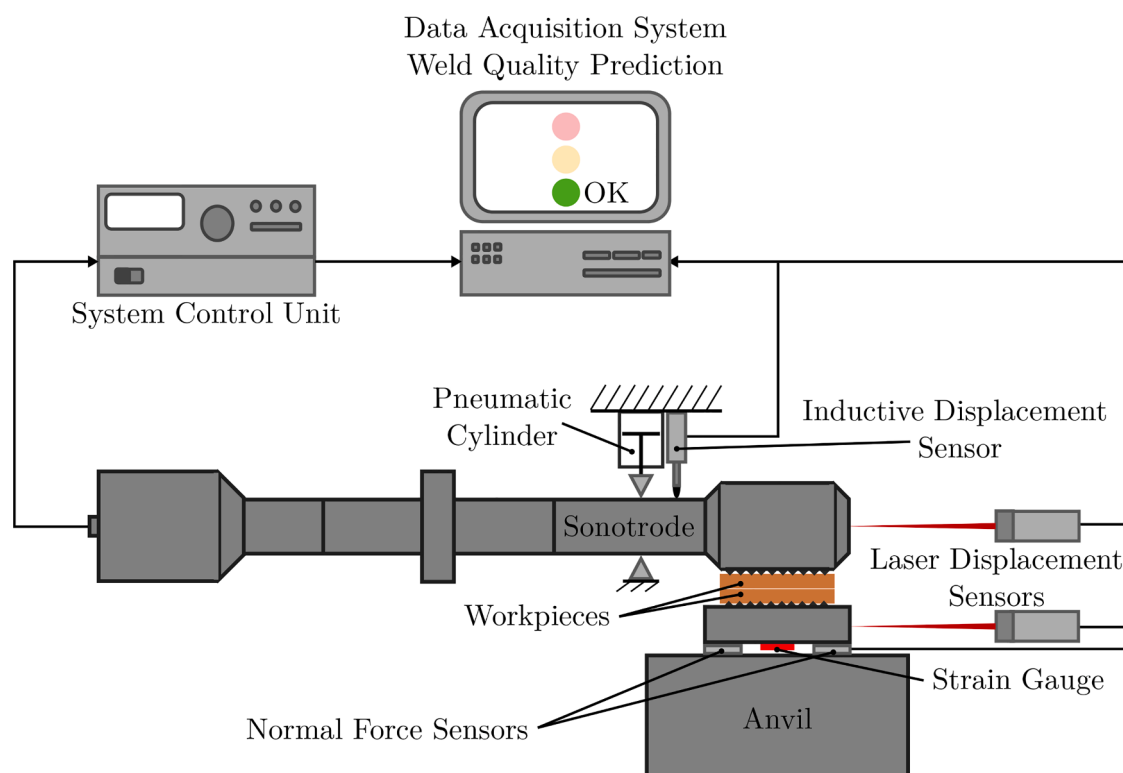


Fig. 1. Machine setup and quality prediction process.

anvil, which provides a better grip on the workpieces.

Figure 3 shows the six-stage model of joint formation proposed by Balz (2020), based on and valid for spot welds of two copper sheets. The relative movements of sonotrode, workpieces and anvil change during the different phases of the welding process. The workpieces remain in the solid state throughout the entire process. Typical process temperatures are between 0.4 and 0.6 times the respective workpiece melting temperature (Balz, 2020; Balz et al., 2020; Gester et al., 2021), thus avoiding common geometrical and metallurgical problems of fusion welding processes, such as porosity, embrittlement or cracking. In addition, the low process temperatures result in the aforementioned minimal formation of brittle intermetallic compounds in dissimilar metal welds. The six-phase model is based on high-speed video measurements. The first phase of the process is characterized by large interfacial motions between the sonotrode and the upper workpiece, as well as between the workpieces themselves. While there is a significant temperature rise, cold deformation still predominates in the joining zone, which is limited to small microcontacts. Analogous to the cleaning phases described in other literature, the second process phase is characterized by shearing and cleaning (de Vries, 2004; Wodara and Adam, 2004). Here, elevated temperatures lead to limited evaporation of impurities and oxide layers and shearing of roughness peaks, resulting in bare metal contact. Subsequent phases three, four and five are characterized by thermal softening and plastic deformation. Welding energy is increasingly transferred in the areas between the sonotrode and the upper workpiece, as well as the lower workpiece and the anvil. In phase five, the joint area has reached its maximum. The differences between the phases are characterized by changes in the microstructure of the joint zone. With increasing energy input, over-welding occurs in the final, the sixth phase of the process (Balz, 2020). If too much energy is introduced in the weld area it starts to soften and, from a certain point, will weaken the joint (Balz, 2020).

USMW processes are controlled by a fixed set of welding parameters, which include the pressure/force applied by the sonotrode, the amplitude of the sonotrode oscillation and a weld termination criterion. The welding power (electrical power required by the transducer) is time-dependent and affected by the damping of the sonotrode oscillation,

which in turn depends on the joint formation and friction losses. The weld termination criterion is given either by the elapsed welding time, a defined welding energy consumption, or by reaching a predefined penetration depth of the sonotrode into the workpieces. The latter is due to softening and plastic deformation. Since only one parameter is usually used to define the end of the weld, the other two variables can be used to monitor the process. However, only monitoring of, e.g., welding time and penetration depth in an energy controlled process has proven to be insufficient to detect or even prevent relevant process variations in industrial applications (Adam et al., 2004; Müller et al., 2022; de Vries, 2004). The parameters for a specific welding process are determined using statistical design of experiments (Elangovan et al., 2010; Heinz et al., 2012; Pauleser et al., 2016; Poovannan, 2015), machine learning based algorithms (Meng et al., 2020; Mongan et al., 2020; Zhao et al., 2017a) and especially concerning the definition of boundary conditions, such as sonotrode and anvil knurling and clamping system skill and experience of the process engineer.

A large number of variables that affect the USMW process and cause the variations mentioned above have been described and studied previously. All variables interact with each other in terms of joint formation and the weld that can be achieved. For a better overview, the influences are divided into machine-dependent and workpiece-dependent influences (Wodara and Adam, 2004).

Most machine-dependent influences do not change without operator intervention. These include machine setup and welding parameters. Frequency and maximum welding power are usually machine-specific as they depend on the generator, the transducer and the natural frequencies of the booster and sonotrode. Increasing the normal force applied by the sonotrode on the workpieces and welding energy, will increase the strength of the joint. After reaching certain optimum values, thermal and mechanical loads lead to over-welding phenomena and joint quality decreases. Wodara and Adam (2004), Balz (2020), de Vries (2004), Al-Sarraf and Lucas (2012). When welding to a predetermined welding energy, the welding time is strongly correlated with the welding force acting perpendicular to the sonotrode oscillations. Zäh et al. (2002), Al-Sarraf and Lucas (2012). The frictional conditions in the joining zone and therefore the required welding power are determined

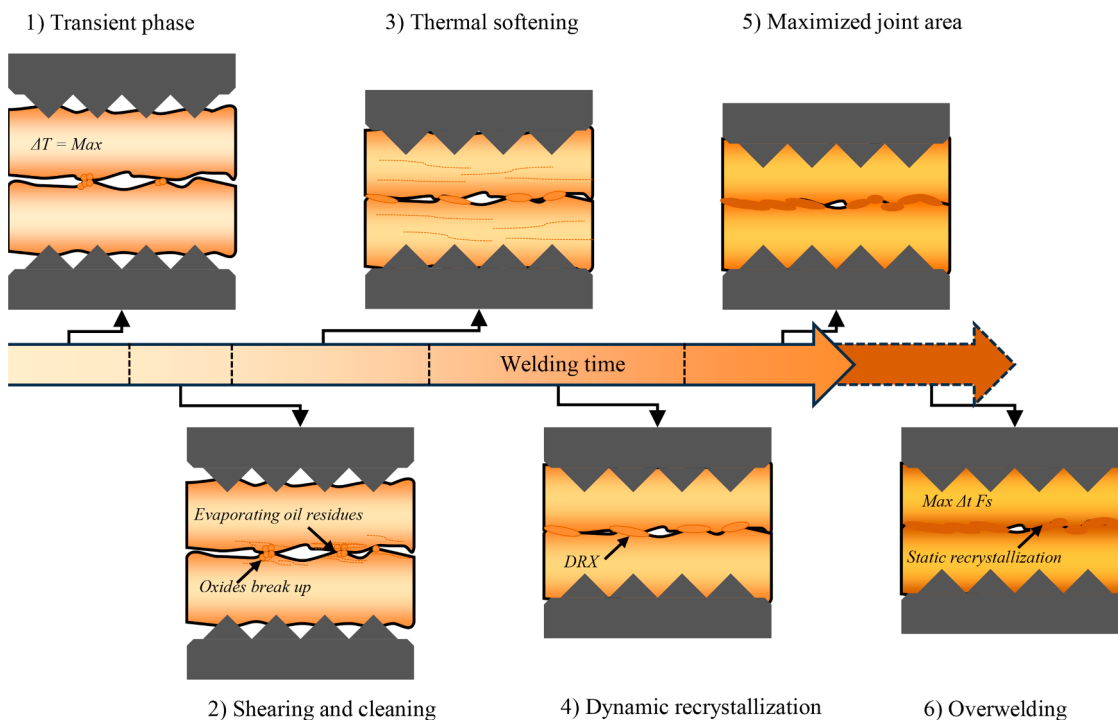


Fig. 3. Process stages and relative movements of parts and joint formation of sheet metal welds according to Balz (2020).

by this very force. It is also important to emphasize the role of the sonotrode oscillation amplitude, which has a strong influence on the relative velocities between the workpieces (Al-Sarraf and Lucas, 2012; DiFinizio, 2005; Wodara and Adam, 2004; Zäh et al., 2002). The booster, sonotrode and anvil are part of the machine setup and are changed periodically, either to set up the machine for different workpieces or to replace worn tools. Tool wear can be considered a long-term disturbance of the process, whereas the adhesion of material to the tool surface, which occurs particularly with aluminum, is more of a short-term or sporadic disturbance. Sonotrode and anvil are defined not only by their material and the size and basic geometry of the weld surface, but also by the exact design of the knurl pattern of the weld surface and any protective coatings (Adam et al., 2004; Wodara and Adam, 2004). Knurling influences the frictional conditions to such an extent that deviations in the welding process can be observed, such as a variation in the welding time (Lu et al., 2016) or, in the case of multi-layer welds, the starting point (Lee, 2013a) of the joint formation. In the case of workpiece influences, deviations from the exact reference state represent disturbances in the welding process, with a significant effect on joint formation and strength. Depending on the selected welding configuration, even the smallest changes can have a considerable influence on the achievable process variation as, e.g., critical natural frequencies of the workpieces may be excited (Müller et al., 2022). Since the workpiece characteristics usually cannot be adjusted (exactly) for each individual weld, they represent a disturbance for each individual welding process. The geometry of the upper workpiece affects the damping of the vibration by the thickness and mass (Rozenberg, 1973; de Vries, 2004; Wodara and Adam, 2004). In addition, the resonance behavior of the workpiece, characterized by length, width and clamping, significantly influences the welding process (Müller et al., 2022; Rozenberg, 1973; de Vries, 2004; Wodara and Adam, 2004). Reducing the thickness of the upper workpiece usually results in a significantly reduced energy requirement, as otherwise over-welding occurs (Müller et al., 2022). Thickness also affects the resistance to penetration of the tool knurls into the components. Similarly, the hardness of the workpiece material has a significant influence on the welding process and the strength of the joint (Adam, 1999; Greitmann et al., 2003; Harthoorn, 1978; Müller et al., 2019; Wodara and Adam, 2004). At this point we would also like to refer to the models of joint formation, in which elastic and plastic deformation play an important role. Since the first phases of the USMW process are characterized by the relative motion between the workpieces and the welding process as a whole is characterized by minimal mixing of the interfaces, the smallest changes in the surface quality have a major impact on the joint quality (Balz, 2020; Wodara and Adam, 2004). To a certain extent, surface impurities and oxides are displaced from the joint zone during the cleaning phase of the welding processes (Balz, 2020; Lee et al., 2014). Nevertheless, the surface structure, cleanliness and overall layer structure, such as oxide layers, adsorbed water and gases, (ingrained) rolling oil residues or coatings, play an important role (Adam et al., 2004; Balz, 2020; Harthoorn, 1978; Lee, 2013b; Wodara and Adam, 2004). The rolling direction can also have a significant influence on the welding process (Balz, 2020), which does not necessarily affect the joint quality (Müller et al., 2022).

Monitoring of ultrasonic metal welding processes

There are two main motivations for observing and measuring USMW processes. On the one hand, there is a strong interest in basic research to investigate and improve the understanding of joint formation, welding process and influence interactions. On the other hand, there is a strong interest in industry- and application-oriented research to predict the quality of a weld and to monitor ongoing production, which is subject to a large number of influencing factors. The different objectives are also reflected in the equipment used for process monitoring. In serial production, the above-mentioned statistical evaluation and monitoring of machine-internal parameters (e.g. resulting welding time and depth) is

well established (DiFinizio, 2005; Greitmann et al., 2003). However, some researchers claim that internal monitoring solutions do not provide accurate and reliable results (Balz, 2020; Balz et al., 2020; de Vries, 2004). An earlier study shows that the influences of material hardness, roughness and weld position overlap all influence welding time and welding depth in an energy controlled process. Since these effects can cancel each other out but can lead to very different weld qualities, monitoring the USMW process only using these scalar values is not feasible (Müller et al., 2022)

For scientific studies of joint formation or the influence of individual variables, such as the surface roughness, measurements using high-speed cameras (Balz, 2020; Balz et al., 2019) and laser vibrometers (Gester et al., 2021; Lu et al., 2016) are state of the art. Often two (Balle et al., 2009; Balz, 2020; Balz et al., 2020; 2019; Kim et al., 2011) or more (Gester et al., 2021; Lu et al., 2016) laser vibrometers are used to determine the relative and absolute oscillations of sonotrode, anvil or workpieces simultaneously. Investigations with laser vibrometers show, that during the welding process oscillations occur not only at the excitation frequency, but also in other frequency ranges. In addition to the expected harmonics, i.e. multiples of the excitation frequency, isolated secondary frequency bands (Gester et al., 2021) occur during the welding process. Depending on the weld configuration, their formation indicates a change in the relative motions. Sensors that measure directly in the process but influence the bond formation or machine stiffness are thermocouples (Balz, 2020; Balz et al., 2020; Gester et al., 2021; Zhao et al., 2017b) and force sensors (Balz, 2020; de Vries, 2004). However, since laser vibrometers and high-speed cameras require a complex setup, an unobstructed view of the process (accessibility/installation space) and high investments in material and personnel qualification, they are not suitable for industrial process monitoring. Balz (2020), Balz et al. (2020). In addition, several studies report poor signal-to-noise ratios or interferences due to particle and vapor formation (Balz et al., 2020; Gester et al., 2021). Nevertheless, the studies conducted using these instruments show that external sensors often provide more or clearer information about the progress of the individual weld than internal sensors. In particular, the anvil is presented as a candidate measurement position (Balz et al., 2020). The above mentioned studies have shown first results on the relative motions during the USMW, but some of them do not consider the entire mechanical system or contradict each other, especially with regard to the description of the end of the process and the phenomena of over-welding.

Application of machine learning in the context of ultrasonic metal welding

Similar to the use of measurement equipment for process observation, the goal of using machine learning tools in the context of USMW is twofold. Some researchers successfully apply machine learning to model the interaction between process parameters and achievable joint quality, replacing other statistical methods usually applied in the form of design of experiments. For USMW of steel on aluminum, Zhao et al. used a neural network to model and investigate the relationship between process parameters and achievable tensile strengths (Zhao et al., 2017a). The work of Mongan et al. confirms the ability of machine learning to predict the strength of welds between steel and aluminum components (Mongan et al., 2020). Meng et al. demonstrate the ability of machine learning response surface methods to simultaneously optimize welding parameters for multiple load cases, such as shear and peel test forces (Meng et al., 2020). Li et al. (2018) considered the use of a deep neural network architecture to predict the failure load of welded joints in ultrasonic welding of composite materials (plastics). Instead of time series data, the described neural network model uses five process parameters as input data, including annealing temperature, surface condition, welding energy, plunge speed, and trigger force. The model is used to estimate the failure load of joints in a lap shear test as a measure of weld quality. The authors report a maximum relative error of 4.5% on a test data set consisting of 54 specimens. Ahmed et al. used the CART variant

of the decision tree algorithm to predict the weld nugget width in resistance spot welding applications, using eleven design and process parameters as inputs. They further leveraged the interpretability of decision trees to extract informative weldability decision rules from the model (Ahmed and Kim, 2017). The use of machine learning to monitor and predict the achieved weld quality for each individual weld is not very established yet. For resistance spot welding Xing et al. employed a random forest model to predict the quality of cold-rolled mild steel welds. The authors considered time-series data consisting of the root mean square welding resistance per half cycle, defined as the dynamic resistance, as inputs with three weld quality types acting as classification targets. The resistance input was pre-processed by extracting welding time stamps and resistance values from four characteristic points in the resistance curve, as well as resistance gradients in the intermediate segments. With the addition of the average dynamic resistance, its standard deviation and the maximum gradient per curve, the model input vectors comprised ten time series features per weld. Furthermore, inclusion of the process parameters electrode force, welding time and welding current as inputs was investigated. Using the established random forest model, the authors report a classification accuracy of 93.6% without and 98.8% with the inclusion of electrode force, welding time and welding current (Xing et al., 2018). The successful application of machine learning methods for the precise prediction of welding conditions confirms the validity of this approach and suggests its use for the assessment of weld quality in USMW based on measurements from external sensors.

Methodology and materials

In the analysis of their influences on process and joint quality, a distinction can be made between defined process parameters (e.g., welding time or normal force) and process disturbances (e.g., surface contamination, changes in microstructure). The influences of the latter are particularly relevant for the monitoring of production processes (Müller et al., 2019), as they are typically unknown and can change for every weld. Against this background, this study aims to investigate whether an external, but industrially applicable, sensor technology can detect and predict the influence of process disturbances on the weld quality. In order to reproduce their effects on weld quality, typical process disturbances are simulated by selecting appropriate materials, e.g., by varying the rolling process to simulate changes in microstructure due to forming processes, or by adjusting the condition of the workpieces, e.g. by applying reproducible surface contamination or changing the surface roughness. In a previous study, the authors have already described the experimental setup used for the experiments (Müller et al., 2022). Therefore, only a summary of the experimental setup, the welding results and the statistical evaluation of the machine-internal parameters will be given here. However, it is supplemented by new investigations of the temporal development of the joint formation. The influence of welding position, material hardness, rolling direction, surface cleanliness and surface roughness on a spot weld of two copper sheets is investigated in this study. Figure 4 lists the changes made starting from the reference welding process. In real applications, these simulated process disturbances may occur in arbitrary combinations. All

the combinations studied are characterized in the following sections.

Welding setup

The welding experiments were performed on a *Schunk Sonosystems GmbH LS-C* ultrasonic welding machine. The machine setup is shown in Figure 1, detailed information on the machine configuration can be found in Table 1.

The reference specimen consists of two Cu-ETP (CW004A) copper sheets of equal size (according to DIN EN 13599:2014) welded in overlap. Cu-ETP is a typical material for electrical and electronic components (Deutsches Kupferinstitut). The reference material is acquired in the half-hard (HH) rolling condition R240, which corresponds to a nominal tensile strength (R_M) of 240 MPa (measured with $R_M = 256.91$ MPa). The dimensions of the 1 mm thick plates, their rolling direction in the reference state (longitudinal) as well as the overlap and welding position are shown in Fig. 5. The figure also shows the Acrylonitrile Butadiene Styrene (ABS) positioning mask used to ensure a repeatable position of the lower workpiece. No other clamping devices were used in the experiments; the upper workpiece was manually positioned based on markings on the anvil, allowing the workpiece to oscillate during the welding process.

The welding parameters are given in Table 2. They are optimized for the reference configuration by a statistical design of experiments (central composite design) for maximum shear force in a lap shear test. The parameter optimization was conducted in two iterations. In a first iteration, the relevant parameter space was identified by conducting preliminary welds with weld parameters selected based on experience. In a second iteration, a full factorial parameter study was performed based on the previously identified parameter space to determine the optimal welding parameters. The welding parameters welding force and amplitude are given as approximate values based on measurements, as on the welding machine used for the experiments, they are only parametrized as cylinder pressure in bar and relative transducer amplitude in percent.

In the energy-controlled mode, the typical (mean) welding time of the established reference process is about 1170 ms. The joint growth for the reference process is shown in Fig. 6. Each picture represents a weld time increment of 150 ms, starting with (a) at 150 ms and ending with (h) at 1200 ms. A time-controlled process was used to obtain these pictures, but the force and amplitude parameters were not changed. The specimens were welded in a rotated overlap so that they could be tested

Table 1
Configuration of the welding machine used for the experiments.

Component	Configuration
Transducer / Generator	4 kW maximum power / 20 kHz working frequency
Booster	1 x 1:1 booster (newly procured for the experiments, no wear-out)
Sonotrode	λ -half longitudinal, 8 mm x 8 mm working surface (newly procured for the experiments, no wear-out)
Sonotrode knurling	0.9 mm x 90° pyramids (diagonal to oscillation)
Anvil knurling	0.5 mm x 90° pyramids (diagonal to oscillation), truncated by 0.1 mm

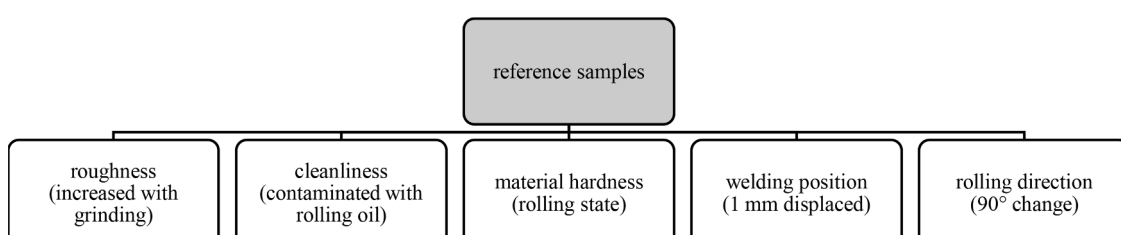


Fig. 4. Overview of variations of reference sample properties.

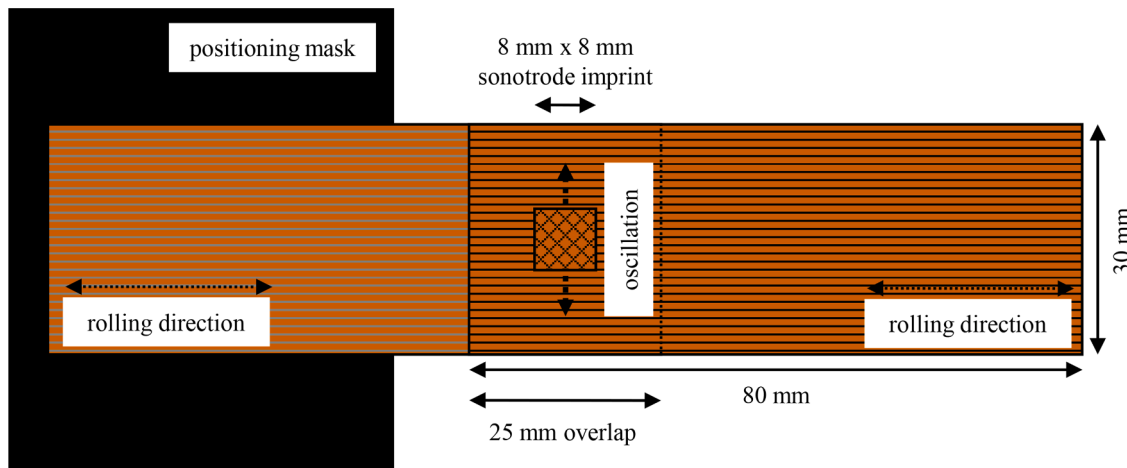


Fig. 5. Work piece geometry and welding position, 80 mm x 30 mm plate size, in 25 mm overlap, rolling direction longitudinal.

Table 2
Welding parameters.

Parameter	Value
Energy	2250 J
Force	≈3000 N
Amplitude	≈25 µm (At the tip of the sonotrode)

destructively by peel testing. This is necessary to obtain optically evaluable surfaces without smearing of the weld surface in the joint zone, as is typical for shear testing. The pictures show the joint surface in the form of peel fracture surfaces. For better visualization, the contrast between the ruptured material and the unjoined surface was increased by controlled oxidation of the welded specimen prior to the peel test. This oxidation was achieved by briefly tempering the specimens in an oven under ambient air. All images show the fracture area of the upper

specimen beneath the sonotrode. The depicted fracture surfaces support the stage models used to describe the welding process (see Fig. 3), with little joined area at the beginning of the welding process.

The first picture (a) at 150 ms welding time shows that, except for isolated joint areas, only the cleaning process has started. The following pictures show the further formation and large-area growth of micro-welds as described in the literature (Adam et al., 2004; Balz, 2020; Wodara and Adam, 2004). The images (a)–(d), taken at welding times of 150 ms to 600 ms, show fracture surfaces with clear contrast. In addition, they show edge areas below the sonotrode working surface that were created during the welding process. These areas are not bonded, but the process brings the plate surfaces sufficiently close together to reduce surface oxidation. It can be seen that the joint growth reaches a maximum at 1050 ms (g) before the typical weld end occurs at 1170 ms, as shown in the image (h) taken at 1200 ms in Fig. 3. The time-dependent growth of the joint surface suggests that monitoring vibrations resulting from forces transmitted across the weld surface may

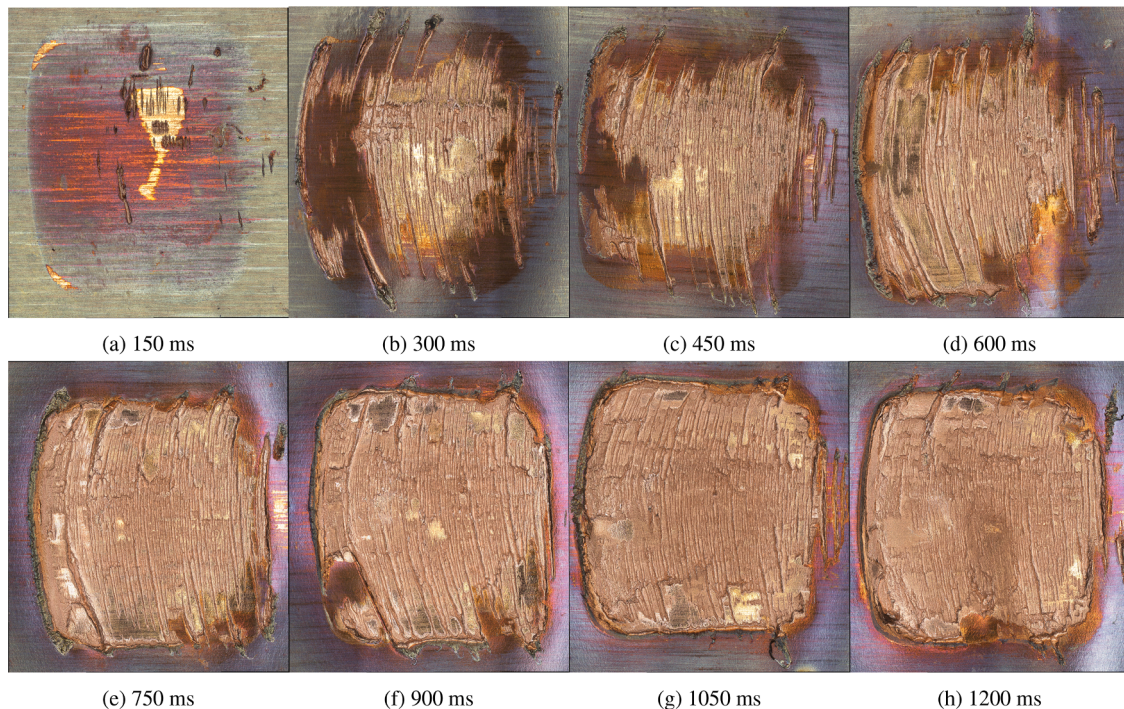


Fig. 6. Formation and growth of joint area, microscopy pictures of peel tested samples. Oxidized prior peeling by short time baking in ambient air in an oven. The welding time was increased from 150 ms to 1200 ms with increments of 150 ms.

represent a promising approach for the weld quality characterization. **Table 3** lists the test series performed and analyzed for this paper. The test series abbreviations refer to their configuration, i.e., the base material strength (e.g., HH - CW004 HH), the rolling direction (e.g., L - longitudinal orientation with the long side of the workpiece as reference), the weld overlap (e.g., P1 - position 1 with 25 mm overlap), and an optional suffix to describe the surface condition. The **Table 3** lists all weld tests with their specific configuration and abbreviations.

Welding results of the test series and quality forecast based on machine-internal data

Table 3 and **Fig. 7** give a statistical overview of the welding results obtained. **Figure 7** shows the maximum shear strength of the welded specimens against the respective welding time as a scatter plot. The welds are grouped according to their configuration and the shear strength of the specimen material. In addition, an individual frequency distribution chart for each group shows the occurrence and dispersion of strength and welding time. While the welds with soft specimen material (S) show a small scatter in both weld time and strength (combined with comparatively low mean values), the welds with hard material (H) show widely scattered values. Some of the configurations, H-L-P1 and H-P-P1, achieve particularly high strengths of 5.4 kN on average, with low welding times and low scatter. In contrast, the strength of the H-L-P2 welds varies between 5.2 kN and 2.2 kN with welding times ranging from 1.1 s to 2.6 s. The half-hard (HH) specimen welds lie between the clusters formed by the hard and soft specimen welds. For all materials, the welds in position P1 are superior to those in P2. Overall, the results show a very large scatter; therefore, from a process engineering point of view, no process capability is given. Since the focus of this paper is on weld quality estimation, a detailed discussion of the weld results and the influencing factors is beyond the scope of this article. **Table 3** shows the mean values and the number of samples within each group, as well as the standard deviations as a percentage of the mean strength, graphically presented in **Fig. 7**. The number of samples refers to the number of welds with a quality label, i.e. a valid maximum shear strength value.

In a previous study, the authors proposed a process monitoring method aimed at predicting the maximum tensile strength of welds using only machine-internal data. This method is based on Gaussian process regression (GPR) with a quadratic kernel using scalar values of weld time and depth as input data (Müller et al., 2022). Furthermore, it was shown that a simple extraction of accessible machine-internal time series data allows feature engineering and a GPR based on these features is able to increase the prediction accuracy without the need for additional external sensor systems (Müller et al., 2022). Specifically, the welding power and sonotrode height measurements sampled at 10 Hz from the welding machine itself were used as the basis for quality prediction (Müller et al., 2022). Here the horn height is used as a measure of

the penetration depth of the horn into the upper workpiece. Scalar features describing the time series data were extracted from the measurements and used to train the GPR with a quadratic kernel. These features include the weld time, the penetration depth, the time and height of the maximum weld power, the curvature of the power curve at the maximum, the increase in weld power during the first 60 ms, and the final welding power and its slope during the last third of the weld. Training the GPR with randomized 2/3 of the data set allows prediction of weld tensile strength with a lowest coefficient of determination R^2 of 0.92 and a highest root mean square error (RMSE) of 266 N. These values represent the worst cases of five random repetitions of data selection and training (Müller et al., 2022). The corresponding average absolute mean error is 198 N, and the absolute median error is 150 N.

Measurement setup

The measurement setup used for the experiments is shown in **Fig. 1**. It consists of two laser displacement sensors (i.e. laser triangulation sensors, LTS), which measure the sonotrode and anvil vibrations (see. **Fig. 8**). In addition, two piezoelectric force sensors connected to a summing box are used to measure the normal forces acting on the anvil. Due to poor accessibility and space limitations, a displacement sensor with a larger measuring range has to be used at the anvil, resulting in a lower resolution compared to the sensor used for the sonotrode. An overview of the specifications is given in the **Table 4**. In addition to these external measurements, a number of machine internal measurements are taken. These include the welding power, the pressure on the pneumatic cylinder that generates the welding force, the welding time and the penetration depth. Due to the poor temporal and spatial resolution of the internal penetration depth sensor, an additional inductive displacement sensor (i.e., a linear variable differential transformer) was mounted directly on the sonotrode support to provide higher resolution measurements.

The selection of this measurement setup is motivated by an cost-effective and easy integration into existing welding machines as used in industry. Against this background, additional measurement technologies have been tested as well, e.g., four strain gauges installed as a full bridge on the backside of the anvil. Due to space limitations, strain gauges cannot be attached on the sides of the anvil (see. **Fig. 8**). Installation of strain gauges on the knurled work surface at the top of the anvil is also not possible. Thus, in this case normal and bending strains cannot be distinguished (superimposed bending). However, for weld quality prediction, vibration and penetration depth measurement have proven to be more suitable, as it will be explained in the following.

Data processing

A high degree of automation in data processing is essential given the

Table 3
Welding experiment test series configuration and results.

Test Series	Base Material Strength [MPa]	Rolling Direction	Overlap [mm]	Surface	Number of Samples	Mean Strength [N]	Standard Deviation s[%]
HH-L-P1 (reference)	256.91	longitudinal	25	clean	235	4176	9.1
HH-L-P2	256.91	longitudinal	26	clean	100	3110	11.0
HH-P-P2	256.91	perpendicular	26	clean	50	3072	10.5
HH-L-P1-o	256.91	longitudinal	25	contaminated	80	2904	16.5
HH-L-P1-rf	256.91	longitudinal	25	rough finish	58	4166	12.3
HH-L-P1-sf	256.91	longitudinal	25	smooth finish	58	4486	5.9
H-L-P1	304.66	longitudinal	25	clean	91	5394	5.6
H-L-P2	304.66	longitudinal	26	clean	62	3518	25.4
H-P-P1	304.66	perpendicular	25	clean	54	5436	2.8
H-P-P2	304.66	perpendicular	26	clean	49	3271	12.2
S-L-P1	231.64	longitudinal	25	clean	97	3184	5.2
S-P-P2	231.64	perpendicular	26	clean	50	2491	3.3
S-L-P2	231.64	longitudinal	26	clean	50	2719	6.0

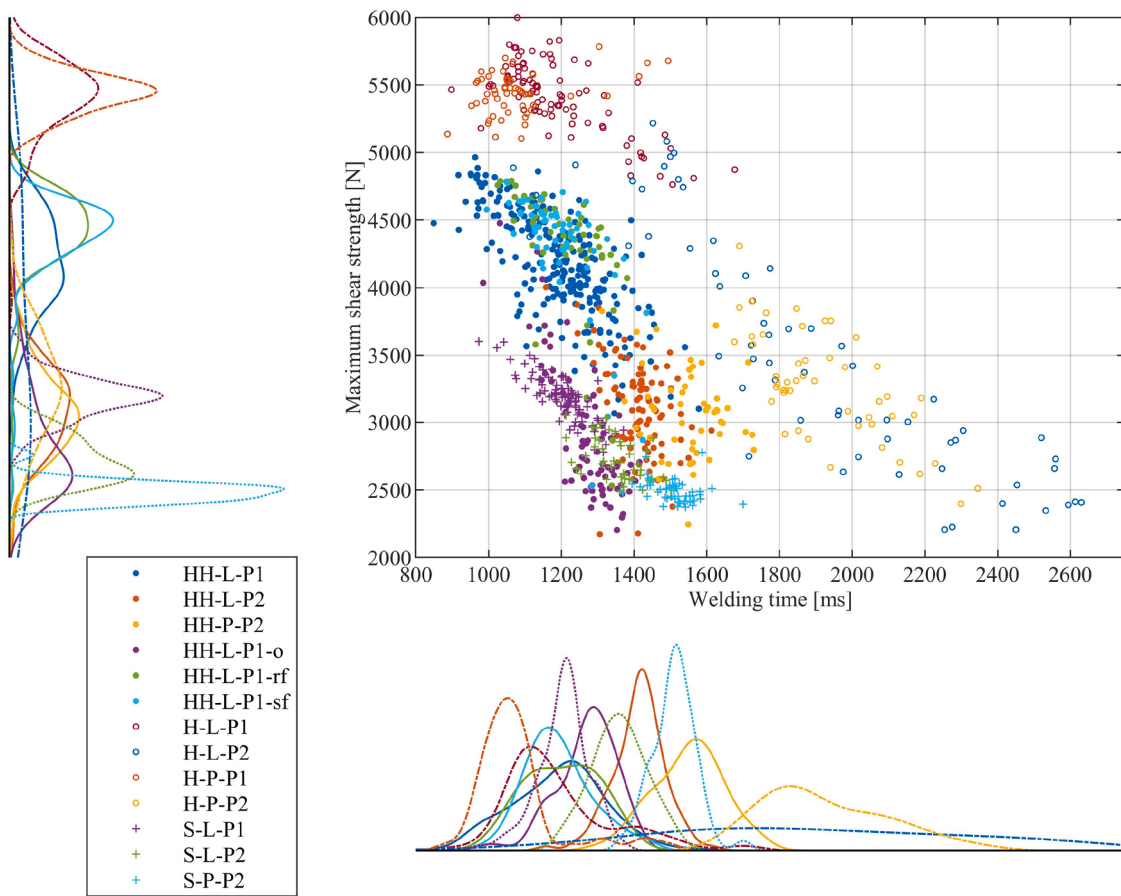


Fig. 7. Overview of the achieved shear strength and weld time.

Table 4
Sensor specifications.

Measured Quantity	Distance	Normal Force	Penetration Depth
Position	Sonotrode	Anvil	Anvil
Measuring distance	20 mm	50 mm	-
Measuring range	0.6 mm	1.2 mm	0 - 26 kN
Sample Frequency	200 kHz	125 kHz	125 kHz
Tolerance	$\pm 1.2 \mu\text{m}$	$\pm 4 \mu\text{m}$	1 %
			$\pm 1.2 \mu\text{m}$

large number of measurements and the goal of transferring the presented methods to industrial applications. In the case of the welding machine used in our experiments, it is not possible to have a precise signal to trigger data acquisition at the start of the welding process. Only the signal indicating the beginning of the sonotrode's downward motion towards the workpiece is available. However, the time between the start of the descent and the start of the welding process is not constant. Therefore, all measurements must be synchronized prior to the analysis. Due to the small welding amplitude and the comparatively low resolution of the displacement sensors, the measurement noise does not allow a gradient based method to determine the beginning of the sonotrode oscillation amplitude increase and thus the beginning of the welding period. Therefore, a method based on the amplitude of the raw signal is used. To this end, an offset correction is performed by subtracting its mean value from the measurement signal. Then, the start of all measurements is synchronized by identifying the first measurement point with an absolute value greater than 80 % of the final weld amplitude and truncating the signal 10 ms before this point. Since the gradient of the sonotrode oscillation amplitude increase is controlled by the welding machine and therefore mostly independent of the surface condition of the workpieces, this method leads to sufficiently accurate results. Both

the laser sensor for measuring the oscillation of the sonotrode and the anvil are driven by the same controller and start recording data at the same time. A similar technique is used for all other sensors except the strain gauge and the penetration depth sensor. For the latter, a gradient based method is used due to the low noise level and high variance in amplitude.

Subsequently, the vibration measurements are transformed into the frequency domain and the amplitude time series at the operating frequency (approximately 20 kHz) and its harmonics (40 kHz, 60 kHz and 80 kHz) are extracted. A steep, almost impulsive increase in amplitude at the beginning of the welding cycle and rapid fluctuations in the measured amplitudes make the continuous wavelet transform the most appropriate method (Daubechies et al., 2011). When using a short-time Fourier transform, the choice of the width of the windowing function has proven to be difficult, taking into account the desired automation of the data processing and the variety of sensors, parameters, frequencies and levels of variance of the measurements.

The continuous wavelet transform compares the signal to a translated and dilated (compressed or stretched) version of a so-called mother wavelet (Daubechies et al., 2011). The dilation factor is typically referred to as the scale. While there is a general correspondence between scale and frequency, there is no precise mapping. Concepts such as the center frequency, calculated by approximating the wavelet with a sine wave, are used to transform from the scale to the frequency domain (Gomez-Luna et al., 2014). Following the methodology proposed by Lilly (2017), generalized Morse wavelets normalized in the time domain by the L^1 norm are used for the continuous wavelet transform. In contrast to the L^2 normalization, which is commonly used in wavelet transforms and guarantees that the wavelet maintains constant energy, the L^1 normalization leads to a more accurate representation of the

amplitudes of the signal [Lilly \(2017\)](#).

The exact sonotrode operating frequency is tuned by the welding machine manufacturer to match the sonotrode's natural frequency and depends on the overall process conditions. Therefore, it deviates slightly from the specified working frequency of 20 kHz and its exact value is unknown. In addition, measurements on the same machine under similar conditions have shown frequency variations during the welding process of 100 Hz around the set value ([Balz, 2020](#)). To account for the operating frequency deviation and variation, a frequency range is defined around the spectral line representing the operating frequency of the sonotrode (e.g. 17 kHz to 23 kHz). For each scale corresponding to a frequency within this frequency range, the sum of all elements in the associated wavelet transform is calculated. Here, synchrosqueezing is applied to improve frequency resolution. Synchrosqueezing is a reallocation method used to sharpen the time-frequency resolution of the wavelet transform ([Daubechies et al., 2011](#)).

Then, the dominant scale with the highest sum is determined and its maximum absolute value of the synchrosqueezed wavelet transform is evaluated. In the next step, all neighboring scales with a maximum absolute value greater than 10% of the dominant scale's maximum are determined and combined into a scale band. Only consecutive scales are considered, i.e., those that are immediate neighbors. A gap in the scale band indicates an additional vibration signal with a frequency similar to the working frequency. Thus, all scales below/above this gap would be neglected. Similar to the studies done by [Daubechies et al. \(2011\)](#), the synchrosqueezed wavelet representation of the vibration measurements has proven to be concentrated about the dominant scale, so that the actual width of the frequency band is insignificant for the results. Finally, the signal is reconstructed from its synchrosqueezed wavelet transform within this scale band (as a complex pointer) and its amplitude is extracted. This process can be considered as an adaptive bandpass filter, where the cut-off frequencies are determined individually for each measurement in order to compensate for the frequency fluctuations caused by the considerable changes in the boundary conditions. The subsequent signal analysis has shown that in the case of the application presented here, the amplitude time series at the working frequency is the most meaningful for the characterization of the weld quality. Therefore, the following studies will focus on the working frequency and neglect its harmonics.

[Figure 9](#) shows a selection of the envelope curves of the anvil oscillations obtained by the synchrosqueezed wavelet transformation. The curves are grouped by configuration and the shear strength obtained for each weld is indicated by the line color. All curves obtained for the sonotrode vibrations (Figure 16) and anvil vibrations (Figure 15), as well as welding power (Figure 17) and penetration depth (Figure 18), can be found in the appendix.

It shall be pointed out that the low amplitudes of the anvil vibrations in the reference configuration ([Fig. 9](#)) at the beginning of the weld formation agree well with the low level of joint formation from the first process steps in Balz's model ([Balz, 2020](#)) and comply with the observations in [Fig. 3](#). The steep inclines of the vibration amplitude as to be

observed for the H-L-P1 configuration shown in [Fig. 9](#) provide new impulses for future work on the topic of joint formation and process stages under different boundary conditions.

Methodology for the prediction of maximum tensile force and defect type from vibration data using machine learning

To predict the quality of a weld with unknown characteristics without physical testing, a supervised machine learning algorithm, the random forest algorithm, is used. Given annotated data from experimental evaluation, machine learning algorithms can learn the complex relationship between sensor data and expected weld quality, as well as the most likely type of process disturbance. The approach presented below does not rely on the time series characteristics specific to each type of sensor data. This is because these vary greatly depending on the welding configuration and sample conditioning, as is evident from Figures 15, 16, 17 and 18. Furthermore, only sensor data that does not require direct inspection of the welded parts was considered as input. Instead, automatic feature extraction and filtering are used, as well as the ability of machine learning algorithms to learn complex relationships.

The random forest algorithm

The random forest algorithm belongs to the family of ensemble learning methods in machine learning and can be used for both classification and regression tasks. By combining a multitude of decision tree learners, the random forest algorithm can produce predictions with reduced variance compared to a single learner, without increasing prediction bias. Each decision tree makes an estimate of the value of the output variable by learning a tree-like structure of simple decision rules over the set of input data features, where each decision is represented by a node in the tree. Given a collection of input vectors \mathbf{X} and corresponding output vectors \mathbf{Y}

$$\mathbf{X} = (\mathbf{x}_1, \dots, \mathbf{x}_K), \mathbf{x}_i = (x_{i,1}, \dots, x_{i,m})^T \in \mathbb{R}^m \quad (1)$$

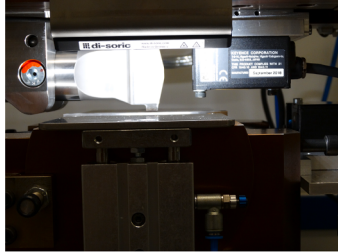
$$\mathbf{Y} = (\mathbf{y}_1, \dots, \mathbf{y}_K), \mathbf{y}_i = (y_{i,1}, \dots, y_{i,n})^T \in \mathbb{R}^n, \quad (2)$$

the algorithm performs a binary split $\theta_N = (f, t_N)$ of the collections of input-output pairs $\mathbf{C} = (\mathbf{x}_i, \mathbf{y}_i) | i \in \{1, \dots, K\}$ based on the value of some input feature f and a threshold t_N defined at Node N , resulting in a left and a right data partition

$$\mathbf{C}_{N,l} = (\mathbf{x}_i, \mathbf{y}_i) | x_{if} \leq t_N \quad (3)$$

$$\mathbf{C}_{N,r} = (\mathbf{x}_i, \mathbf{y}_i) | x_{if} > t_N. \quad (4)$$

The optimal split θ_N^* at the node is then found by minimizing an impurity measure over the data partitions, such as Gini impurity metric or entropy for classification problems and the mean squared output error (MSE) for regression problems ([Gordon et al., 1984](#)). This procedure is



(a) Laser triangulation sensor.



(b) Laser triangulation sensors.



(c) Strain gauges attached to the back of the anvil.

Fig. 8. Welding area, with laser triangulation sensors for vibration measurements at the sonotrode and anvil, as well as the strain gauges attached to the back of the anvil.

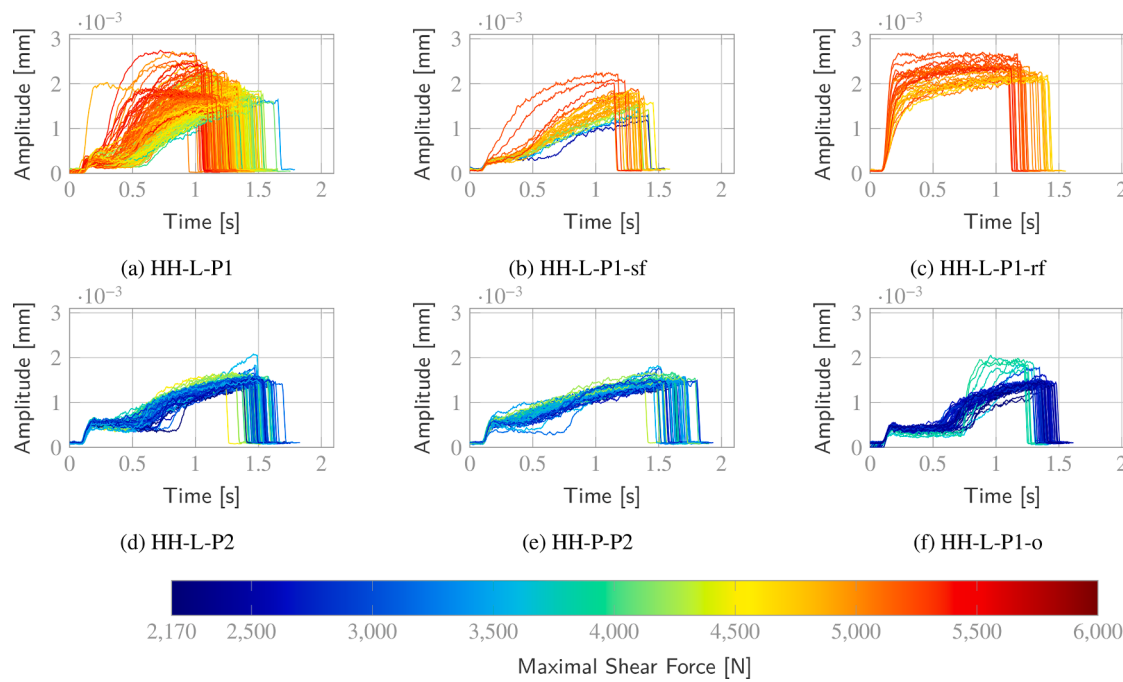


Fig. 9. Exemplary time series of the anvil vibration's amplitude at the working frequency under variation of the boundary conditions.

repeated recursively on the partitions $C_{N,l}, C_{N,r}$ until a termination criterion is met, such as the maximum depth of the tree, or each partition contains only one sample.

The random forest algorithm improves the performance of decision trees by applying bootstrap aggregation to a set of tree models. For each decision tree, a unique training data set is constructed by randomly sampling from the original training data. This ensures that no data element is selected more than once in a training data set. The model is trained using these newly constructed data sets. The prediction of the random forest on a set of test data is then the average of all individual predictions for regression problems, or the majority vote in the case of classification (Breiman, 1996).

Feature extraction

The complexity of the relationship between input and output data is reduced by extracting descriptive features from the time series measurement signals. Not only does this reduce the computational costs of model training, but it also reduces the size of the input data. To identify the most relevant features, a large number of candidate features are computed for each signal type and experiment. These include geometrical and statistical measures such as the mean and median values of the signal, the relative positions of significant change points normalized to the welding time, or measures to access the symmetry of the signal (Fig. 10a). A complete list of features is given in the Table 5. Each feature

is calculated for the original signal and its first two numerically calculated derivatives. In addition, all features are accessed for the complete signals and for a number of equally spaced sections of the signal (Fig. 10c), which greatly increases the number of individual feature values and adds the ability to correlate feature values with welding process phases. In the first step of the training phase, the random forest is trained using all features of the provided inputs, followed by the identification of the (model-dependent) most significant features on the training data set using SHAP (SHapley Additive exPlanations), a game-theoretic approach to explainable machine learning (Lundberg and Lee, 2017). The model is then retrained using the set of significant features and validated on a previously unseen test dataset where only the relevant features are extracted.

The location of the change points is computed by binary segmentation using the Python library ruptures (Truong et al., 2020). The quadratic error loss is used as the cost function for the segmentation, which computes the least squares deviation to detect shifts in the mean of the signal. For curvature estimation, only the first section of the measurement data series (by default 1/6 of the length of the series) is considered. The central point is defined to be at the maximum in this section and the other two at a fixed distance ($\pm 1/12$ of the length of the series) from it in both directions. Before the actual model training, the number of equally spaced sections of the signal, the symmetry threshold r , and the parameters for the curvature calculation are determined in a hyper-parameter optimization. The hyper-parameter optimization is

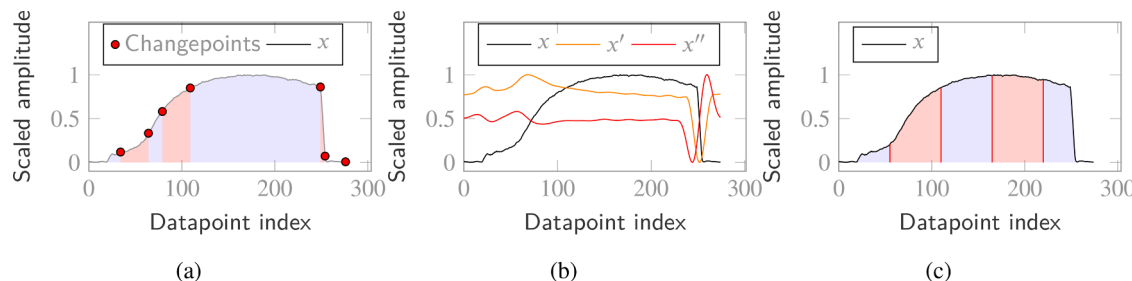


Fig. 10. Change point positions (a) used as features extracted from each signal, numerical differentiation of signals (b) and splitting of a signal into predefined segments (c).

Table 5
Welding experiment test series configuration and results.

Feature	Influential parameters	Description
Length	-	Length of the measurement vector. The sampling frequencies are held constant over all experiments, thus the number of measurement points directly corresponds to the weld time
Maximum value	-	Maximum value of the measurement vector
Minimum value	-	Minimum value of the measurement vector
Sum	-	Sum over the whole measurement vector
Euclidean norm	-	Euclidean norm of the measurement vector
Median	-	Median of the measurement vector
Mean norm	-	Mean of the measurement vector
Symmetry	Threshold value r	Symmetry of the measurement vector x , defined as Boolean variable. True if: $\frac{\ \text{mean}(x) - \text{median}(x) \ }{\max(x) - \min(x)} < r$
Number of significant peaks	Minimal peak height, minimal distance between two consecutive peaks	Number of significant (positive and negative) peaks in the vector, after low-pass filtering
Position of change points	Number of points, detection method, parameters of the detection method	Relative position of the points in the vector that have been identified as change points. Change points can be used for the segmentation of the signal.
Curvature	Choice of points, smoothing method (here running mean)	Using three points, a circle can be parametrized, which is used as an approximation of the curvature of the measurement vector. This proved to be more meaningful than characteristic values based on, e.g., the second derivative. The curvature is evaluated on the smoothed measurement vector for either, every change point section or for a predefined signal section. By default, only the first section of the vector is taken into account, with the central point at the maximum and the two others at a fixed distance from it in both directions.

conducted using a grid search. By far the best SHAP values are attributed to the mean values of the equally spaced sections of the measurement data series (here five sections were chosen) and the total sum over the entire data series.

Stratified K-fold cross-validation

The most common model evaluation process involves two steps. First, the model undergoes a training step in which its parameters are adjusted to achieve optimal prediction performance on a training data set. In the subsequent validation step, the performance of the optimized model is then evaluated on a previously unseen test data set using predefined metrics (Bishop, 2006). This is necessary to estimate how well the model generalizes to new data. However, smaller data sets are often prone to selection bias due to statistical variation, as the validation

result may depend heavily on the choice of training and test data (Goodfellow et al., 2016).

To mitigate this problem, a stratified k-fold cross-validation procedure is used for the validation presented in the latter. Here, the full data set containing all independent samples is divided into k subsets of approximately equal size. In the case of a classification task these subsets contain similar proportions of samples for each target class. Iterating over all subsets, each is then used once for validation, while the remaining subsets are used to train the model, as shown in Fig. 11. The collection of k validation results can then be used to obtain an estimate of the mean prediction performance according to the chosen metrics, allowing a more informative assessment of the quality of the model and its ability to generalize (Goodfellow et al., 2016).

Results and discussion

This section discusses the quality prediction results obtained with the previously presented data acquisition, processing, and machine learning strategies. Two machine learning problems are addressed, quality prediction in the form of tensile shear strength estimation and, for a smaller data set, a welding process disturbance classification.

Prediction of maximum shear force

Using the established training and prediction pipeline, the prediction of the achieved weld strength, measured by the maximum tensile shear force, was evaluated. Both the inclusion of a single measurement signal type and combinations of multiple signal types were considered. The results of these experiments, obtained using a 5-fold cross-validation method (4.3) to account for the relatively small size of the data set, are summarized in Table 6 below. The parameters of the random forest regressor are listed in Table 7. Hyperparameter optimization has shown that there is a minimum number of about 100 trees to get satisfactory results. However, higher numbers of trees lead to better results. Here, 1000 trees were chosen as a compromise between computational cost and prediction accuracy.

As is evident from the numerical results, the anvil oscillation

Table 6

Estimation error for different combinations signal types included in the prediction model. Here, the acronym ANV denotes the anvil vibration amplitude time series signal, STR strain gauge data of the anvil, PEN penetration depth data and POW the welding power time series of the generator.

Datatype	R ²	Mean abs. error [N]	Median abs. error [N]	Mean rel. error [%]	Median rel. error [%]
ANV	0.906	209.21	136.12	5.75	3.73
POW	0.825	259.75	137.69	6.81	3.98
PEN	0.959	154.02	102.59	4.86	3.39
STR	0.595	258.24	215.12	8.62	7.56
ANV & POW	0.939	187.03	125.88	4.90	3.33
ANV & PEN	0.964	137.33	76.03	4.30	2.60
POW & PEN	0.963	138.97	87.82	4.45	2.96

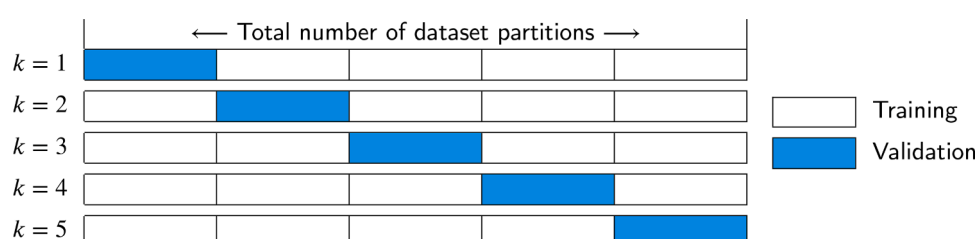


Fig. 11. K-fold cross-validation. Each subset is used exactly once for validation.

Table 7
Random forest parameters.

Parameter	Classification	Regression
Number of trees	1000	1000
Number of features	Number of features	Square root of the number of features
Maximal depth	1000	1000
Minimal number of samples for a split	2	2

amplitude time series signal (ANV) and the penetration data (PEN), with R^2 values of 0.906 and 0.959, respectively, are particularly well suited for use as inputs. The graph of measured shear forces against predicted shear forces for a representative test data set in Fig. 12 confirms these results. However, it can be seen from Fig. 12b that, due to the late inclusion of the high-resolution penetration sensor, there are few samples in the mid-shear force range of 4000 N to 5000 N. As a result, the estimates based on the anvil oscillation data are of greater significance. The results obtained using strain gauge (STR) data (Figure 19b) are significantly worse and were not considered further.

Using different combinations of two of the three most relevant signal types anvil vibration data, power data and penetration data, the previous results could be improved, with the combination of welding power (POW) and anvil vibration data achieving a R^2 of 0.939 with results spanning the entire observed shear force spectrum. A comparison of Fig. 13c with Figures 19a and 12 a shows that this combination significantly reduces the presence of outliers, resulting in lower mean absolute and relative errors as shown in Table 6. Combinations of three or more signal types were considered, but did not result in further improvements.

Classification of weld defects

While predicting the maximum achievable shear force as an indicator of weld quality is particularly relevant for automated sorting of welded workpieces, it does not provide any information about the condition of the workpieces during the welding process (e.g. surface condition, hardness). To evaluate whether it is possible to predict the welding conditions from the collected sensor data, a random forest classifier was trained on the features extracted from the anvil vibration data. Only a subset of the original welding configuration variations (Table 3) was considered (i.e. HH-L-P1, HH-L-P1-o, HH-L-P1-rf, HH-L-P1-sf, H-L-P1, S-L-P1), as including data collected at the shifted welding

position P2 resulted in minority classes with too few samples. This may be due to the high variation in the welding process, as illustrated in Figure 15 (h), and the comparatively small number of experiments. Further experiments would have to be conducted to allow classification on the dataset welded at position P2. The parameters of the random forest classifier are listed in Table 7. The average results obtained with this classification method, again using a 5-fold cross-validation, are shown in Fig. 14a, in the form of a confusion matrix normalized over the true classes.

The classifier was able to clearly separate the different welding conditions, correctly identifying the presence of oil on the surface of the weld material and the preparation of the surface with rough abrasive fabric (HH-L-P1-rf) in all cases. Only the classification of the specimens prepared on the surface with light abrasive cloth (HH-L-P1-sf) shows a classification accuracy below 90%. This can be explained by the apparent similarities between the sensor data collected for this case and the data for the reference case. To evaluate the overall classification accuracy, the macro and micro averages of the F_1 score are assessed. The F_1 score is defined as

$$F_1 = \frac{TP}{TP + \frac{1}{2}(FP + FN)} . \quad (5)$$

Here TP stands for the true positives, FN for the false negatives and FP for the false positives. The macro-averaged F_1 score is the arithmetic mean of all per-class F_1 scores, while the micro-averaged F_1 score is the sum of all true positives, false negatives and false positives. Overall, satisfactory macro and micro average F_1 scores of 94% and 95%, respectively, were achieved. Furthermore, using a one-against-all approach, the receiver operating characteristic (ROC) curve for each class, which illustrates the diagnostic quality of a model as its decision threshold is varied, was examined and a macro- and micro-average ROC curve over all classes was computed. The area under the macro averaged curve was then used as an evaluation metric, as it is independent of the chosen decision threshold and indicates how well the classes are separated by the classifier. With a value of 0.99, the area under the ROC curve further confirms the conclusion that the chosen approach is well suited for the identification of unknown welding conditions from sensor data.

Outlook

The results of this study prove the feasibility of the presented on-line monitoring method for predicting the maximum tensile force of

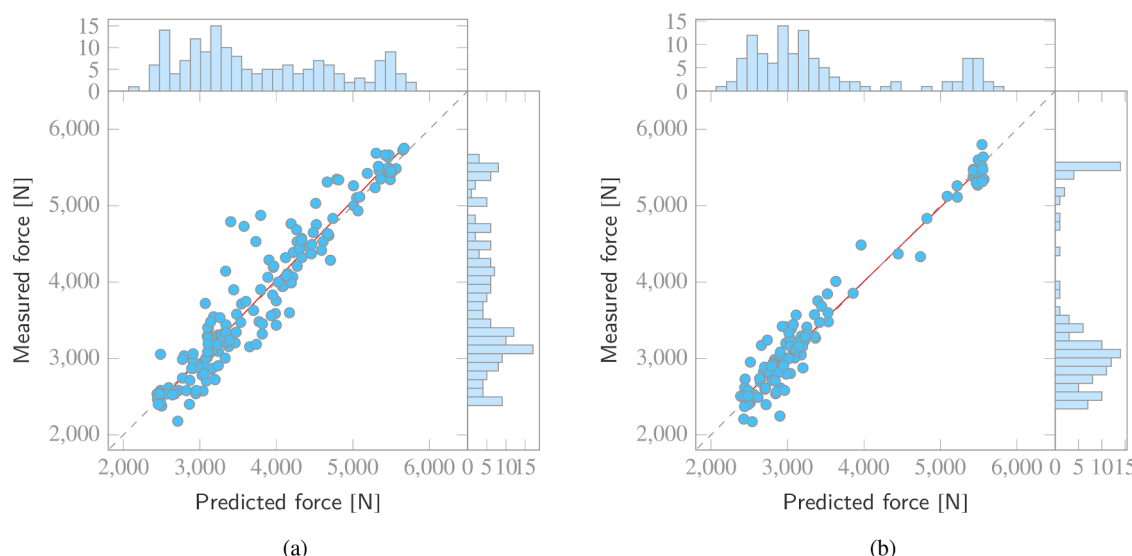


Fig. 12. Prediction results based solely on anvil vibration data (a) or penetration data (b).

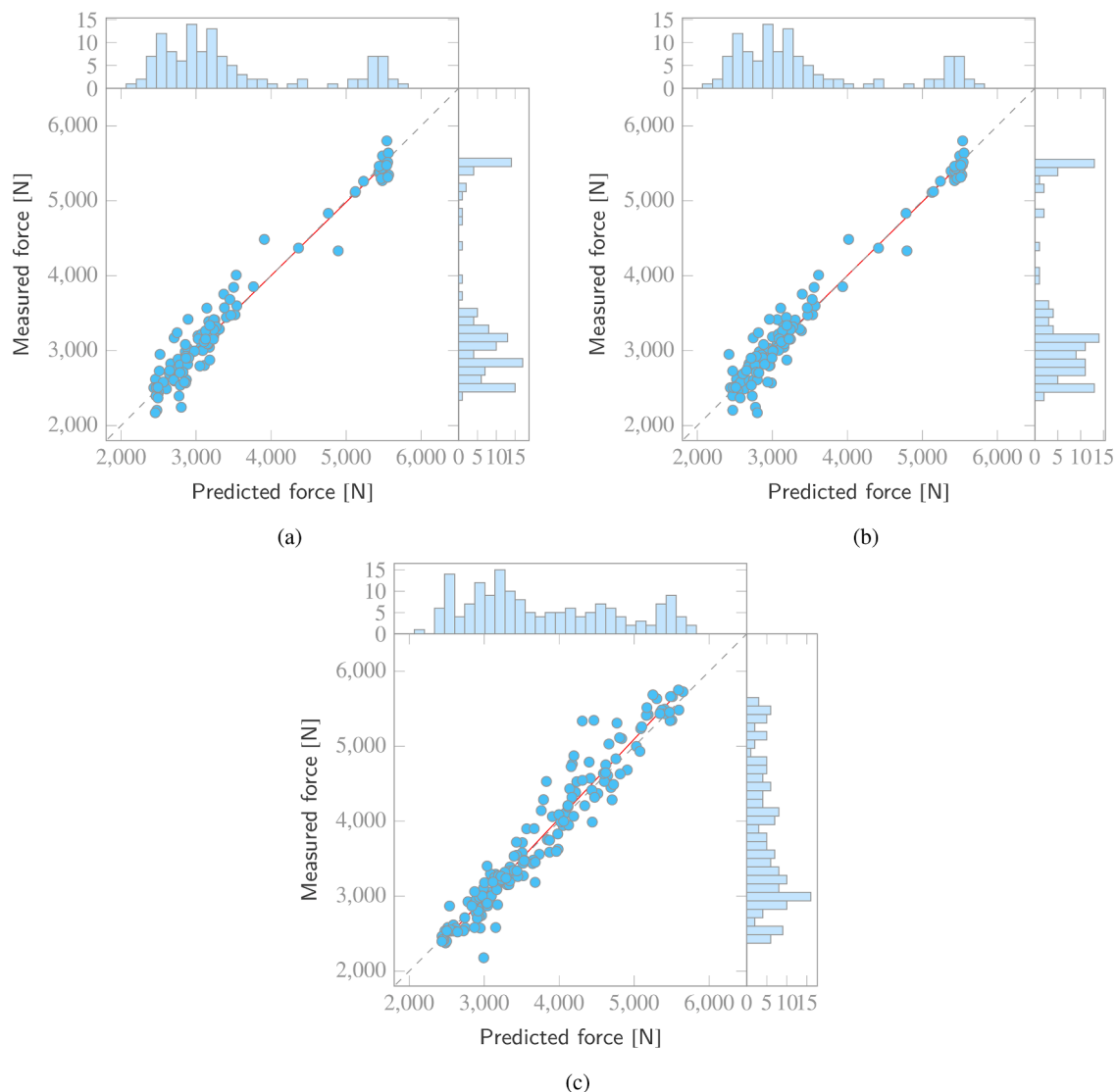


Fig. 13. Prediction results for the combination of anvil vibration and penetration data (a), power and penetration data (b) and power and anvil vibration data (c).

ultrasonic metal welds. The results obtained motivate further research. On the one hand, it should be investigated how well the prediction method can be implemented in a real environment. The results of the study suggest a robust applicability. In the context of real-world applications, a fundamental investigation of stranded wire terminal connections is also interesting (Gester et al., 2021). From the research perspective, however, it is particularly interesting to investigate which conclusions can be drawn from the identified features and the random forest model with respect to joint formation. Within the scope of this research project, similar results were obtained with the specimen material aluminum (EN AW1050A) (Müller et al., 2022).

Conclusion

In summary, it can be concluded that it is possible and reasonable to monitor the USMW using external measurements, especially when vibration and penetration depth measurements are considered. Different monitoring methods have been successfully tested. Possible sensor setups for different applications were validated and characterized for their suitability for monitoring. Significant signal features were identified and a method for automated signal processing was implemented. It should be emphasized that the analysis of the oscillations at the operating frequency in the range of 20 kHz already provides the relevant

information for the formation of the joint. The quality of the data obtained from the various measurement signals is particularly noteworthy. The results indicate, that welding power, penetration depth and anvil vibration measurements are particularly valuable sources of information for the welding configurations studied here. Taking into account the anvil vibration and the penetration depth, a regression model with a R^2 value of 0.964 and a mean relative estimation error on the shear strength of 4.30% could be established. Taking into account the internal power curve and the penetration depth, a slightly less accurate regression model with a R^2 value of 0.963 and a mean relative estimation error of 4.45% could be obtained. These results far exceed the usual established process monitoring methods on M-USS machines. In this context, the laser triangulation sensor used to detect the anvil oscillation can also be replaced by alternative measurement technologies, such as eddy current sensors. The robustness of the quality prediction using random forest algorithms suggests that the developed methods can be transferred to other welding configurations. Validation of the selected measurement technology and adaptation of the data preparation to the welding process is necessary for the particular application before quality prediction or classification can be learned.

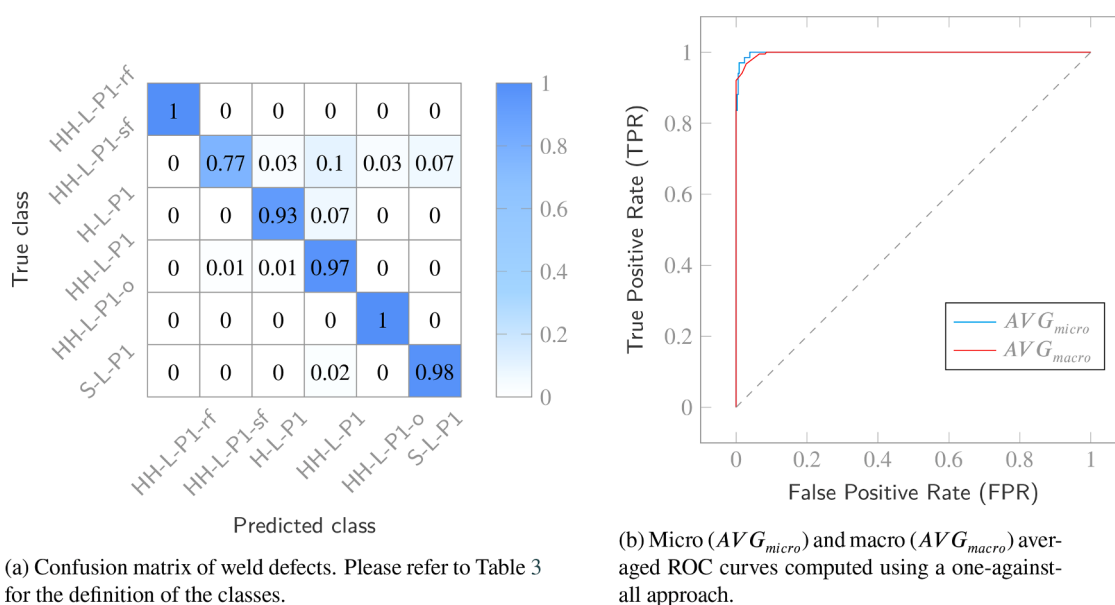


Fig. 14. Confusion matrix of weld defect class prediction normalized over the true classes (a) and averaged ROC curves (b) using the random forest algorithm.

CRediT authorship contribution statement

Florian W. Müller: Data curation, Writing – original draft. **Christian Mirz:** Data curation, Formal analysis, Writing – original draft. **Sascha Weil:** Formal analysis, Writing – original draft. **Alexander Schiebahn:** Supervision. **Burkhard Corves:** Supervision. **Uwe Reisgen:** Supervision.

Declaration of Competing Interest

The authors declare that they have no known competing financial interests or personal relationships that could have appeared to influence the work reported in this paper.

Data availability

Data will be made available on request.

Acknowledgments

The IGF project “Systemidentifikation und Monitoring von Metall-Ultraschallschweißprozessen”, IGF project no. 20.161 N, of the Research Association “Schweißen und verwandte Verfahren e. V.” of the DVS, Aachener Str. 172, 40223 Düsseldorf, Germany, was funded by the Federal Ministry for Economic Affairs and Energy via the AiF within the framework of the program for the promotion of joint industrial research (IGF) on the basis of a resolution of the German Bundestag.

Funded by the Deutsche Forschungsgemeinschaft (DFG - German Research Foundation) under Grant Number 520475171 ‘Hybrid Process Prognosis for Metal Ultrasonic Welding - Pro²MUSS’.

Supplementary material

Supplementary material associated with this article can be found, in the online version, at [10.1016/j.jajp.2023.100149](https://doi.org/10.1016/j.jajp.2023.100149).

References

- Adam, T., Martinek, I., Wodara, J., 2004. Einsatz des Ultraschall-Metallschweißens für innovative Werkstoffe und interessante Problemstellungen der Wirtschaft. In: DVS-Berichte, Vol. 232. DVS-Verlag, Düsseldorf.
- Agency, I.E., Global EV outlook 2021: accelerating ambitions despite the pandemic. <https://iea.blob.core.windows.net/assets/ed5f4484-f556-4110-8c5c-4ede8bcba637/GlobalEVOutlook2021.pdf>.
- Ahmed, F., Kim, K.-Y., 2017. Data-driven weld nugget width prediction with decision tree algorithm. Procedia Manuf. 10, 1009–1019. <https://doi.org/10.1016/j.promfg.2017.07.092>.
- Al-Sarraf, Z., Lucas, M., 2012. A study of weld quality in ultrasonic spot welding of similar and dissimilar metals. In: Conference Series (Online), Vol. 382. IOP Publishing Ltd.
- Balle, F., Wagner, G., Eifler, D., 2009. Charakterisierung des ultraschallschweißprozesses durch hochauflösende laser-doppler-vibrometrie. InFocus – Magazin für Optische Messsysteme (1).
- Balz, I., 2020. Prozessanalyse der thermo-mechanischen Vorgänge während der Verbindungsbildung beim Metall-Ultraschallschweißen. In: Aachener Berichte Fügetechnik, 1. auflage, Vol. 2020.3. Shaker, Düren.
- Balz, I., Raad, E.A., Rosenthal, E., Lohoff, R., Schiebahn, A., Reisgen, U., Vorländer, M., 2020. Process monitoring of ultrasonic metal welding of battery tabs using external sensor data. J. Adv. Joining Process. 1, 100005. <https://doi.org/10.1016/j.jajp.2020.100005>.
- Balz, I., Rosenthal, E., Reimer, A., Turiaux, M., Schiebahn, A., Reisgen, U., 2019. Analysis of the thermo-mechanical mechanism during ultrasonic welding of battery tabs using high-speed image capturing. Welding World 63 (6), 1573–1582. <https://doi.org/10.1007/s40194-019-00788-z>.
- Bansal, P., Kockelman, K.M., 2017. Forecasting americans’ long-term adoption of connected and autonomous vehicle technologies. Transp. Res. Part A Policy and Pract. 95, 49–63. <https://doi.org/10.1016/j.tra.2016.10.013>.
- Bergmann, J.P., Regensburg, A., Schürer, R., Petzoldt, F., Herb, A., 2017. Effect of the interface characteristics on the joint properties and diffusion mechanisms during ultrasonic metal welding of Al/Cu. Welding World 61 (3), 499–506.
- Bishop, C.M., 2006. Pattern Recognition and Machine Learning (Information Science and Statistics). Springer-Verlag, Berlin, Heidelberg.
- Breiman, L., 1996. Bagging predictors. Mach. Learn. 24 (2), 123–140. <https://doi.org/10.1007/BF00058655>.
- Daubechies, I., Lu, J., Wu, H.-T., et al., 2011. Synchrosqueezed wavelet transforms: an empirical mode decomposition-like tool. Appl. Comput. Harmon. Anal. 30 (2), 243–261. <https://doi.org/10.1016/j.acha.2010.08.002>.
- Deutsches Kupferinstitut, e. V., Werkstoff-datenblätter - cu-ETP.
- DiFinizio, T., 2005. Ultrasonic intelligence. Wire Cable Technol. Int. 33 (5), 88–90.
- Elangovan, S., Prakasan, K., Jaiganesh, V., 2010. Optimization of ultrasonic welding parameters for copper to copper joints using design of experiments. Int. J. Adv. Manuf. Technol. 51 (1-4), 163–171. <https://doi.org/10.1007/s00170-010-2627-1>.
- Gester, A., Wagner, G., Pöthig, P., Bergmann, J.P., Fritzsche, M., 2021. Analysis of the oscillation behavior during ultrasonic welding of EN AW-1070 wire strands and EN CW004a terminals. Welding World. <https://doi.org/10.1007/s40194-021-01222-z>.
- Gomez-Luna, E., Aponte, G., Pleite, J., 2014. Application of wavelet transform to obtain the frequency response of a transformer from transient signals-Part II: practical assessment and validation. IEEE Trans. Power Deliv. 29, 2231–2238. <https://doi.org/10.1109/TPWRD.2013.2295377>.
- Goodfellow, I., Bengio, Y., Courville, A., 2016. Deep Learning. MIT Press.<http://www.deeplearningbook.org>

- Gordon, A.D., Breiman, L., Friedman, J.H., Olshen, R.A., Stone, C.J., 1984. Classification and regression trees. *Biometrics* 40 (3), 874. <https://doi.org/10.2307/2530946>.
- Greitmann, M.J., Adam, T., Holzweißig, H.G., Stroh, D., Wagner, G., Wiesner, P., Züst, R., 2003. Gegenwärtiger stand und zukunftsansichten der sonderschweißverfahren - ultraschallschweißen. *Schweißen und Schneiden* 55 (6).306–308, 310, 312–314
- Hartoorn, J.L., 1978. Ultrasonic metal welding. *Technische Hogeschool Eindhoven*, Eindhoven. Dissertation.
- Heinz, S., Wagner, G., Eifler, D., 2012. Ultrasonic welding of wires and cables. *JOM* 64 (3), 421–426. <https://doi.org/10.1007/s11837-012-0266-8>.
- Kim, W., Argento, A., Grima, A., Scholl, D., Ward, S., 2011. Thermo-mechanical analysis of frictional heating in ultrasonic spot welding of aluminum plates. *Proc. Inst. Mech. Eng. Part B (J. Eng. Manuf.)* 225 (7), 1093–1103.
- Köhler, T., Raab, M., Regensburg, A., Bergmann, J.P., 2019. Liquid interlayer formation during torsional ultrasonic welding of EN CW004a and EN AW1050. *Welding World*. <https://doi.org/10.1007/s04194-019-00763-8>.
- Lee, S., 2013. Process and quality characterization for ultrasonic welding of lithium-ion batteries. University of Michigan, Michigan. Dissertation.
- Lee, S., 2013. Process and quality characterization for ultrasonic welding of lithium-ion batteries. University of Michigan. Dissertation.
- Lee, S.S., Shao, C., Kim, T.H., Hu, S.J., Kannatey-Asibu, E., Cai, W.W., Spicer, J.P., Abell, J.A., 2014. Characterization of ultrasonic metal welding by correlating online sensor signals with weld attributes. *Trans. ASME J. Manuf. Sci. Eng.* 136 (5), 051019/1–10.
- Li, Y., Lee, T.H., Wang, C., Wang, K., Tan, C., Banu, M., Hu, S.J., 2018. An artificial neural network model for predicting joint performance in ultrasonic welding of composites. *Procedia CIRP* 76, 85–88. <https://doi.org/10.1016/j.procir.2018.01.010>.
- Lilly, J.M., 2017. Element analysis: a wavelet-based method for analysing time-localized events in noisy time series. *Proc. Math. Phys. Eng. Sci.* 473 (2200), 20160776. <https://doi.org/10.1098/rspa.2016.0776>.
- Lu, Y., Song, H., Taber, G.A., Foster, D.R., Daehn, G.S., Zhang, W., 2016. In-situ measurement of relative motion during ultrasonic spot welding of aluminum alloy using photonic doppler velocimetry. *J. Mater. Process. Technol.* 231, 431–440.
- Lundberg, S.M., Lee, S.-I., 2017. A unified approach to interpreting model predictions. In: Guyon, I., Luxburg, U.V., Bengio, S., Wallach, H., Fergus, R., Vishwanathan, S., Garnett, R. (Eds.), *Advances in Neural Information Processing Systems 30*. Curran Associates, Inc., pp. 4765–4774. <http://papers.nips.cc/paper/7062-a-unified-approach-to-interpreting-model-predictions.pdf>
- Meng, Y., Rajagopal, M., Kuntumalla, G., Toro, R., Zhao, H., Chang, H.C., Sundar, S., Salapaka, S., Miljkovic, N., Ferreira, P., Sinha, S., Shao, C., 2020. Multi-objective optimization of peel and shear strengths in ultrasonic metal welding using machine learning-based response surface methodology. *Math. Biosci. Eng. MBE* 17 (6), 7411–7427. <https://doi.org/10.3934/mbe.2020379>.
- Mongan, P.G., Hinchy, E.P., O'Dowd, N.P., McCarthy, C.T., 2020. Optimisation of ultrasonically welded joints through machine learning. *Procedia CIRP* 93, 527–531. <https://doi.org/10.1016/j.procir.2020.04.060>.
- Müller, F.W., Schiebahn, A., Reisgen, U., 2019. Untersuchungen zum störeinfluss von werkstoff- und oberflächeneigenschaften auf cu-cu metall-ultraschallschweißverbindungen. *METALL* 73 (419 der Gesamtfolge), 464–467.
- Müller, F.W., Schiebahn, A., Reisgen, U., 2022. Quality prediction of disturbed ultrasonic metal welds. *J. Adv. Joining Process.* 5, 100086. <https://doi.org/10.1016/j.jajp.2021.100086>.
- Müller, F.W., Mirz, C., Weil, S., Reisgen, U., Schiebahn, A., Corves, B., 2022. Systemidentifikation und monitoring von metall-ultraschallschweißprozessen. *Schweißen und Schneiden* 5, 2231–2238.
- Pauleser, T., Vorholt, F., Mayer, B., Essers, M., Schiebahn, A., Reisgen, U., Schmidt, P., Theodossiadis, G., Zäh, M.F., 2016. Elektrische kontaktierung von lithium-ionen-batterien für den einsatz in elektro- und hybridfahrzeugen: Produktionsforschung zu hochvoltspeichersystemen für die elektromobilität : Verbundprojekt. In: Allmann, C. (Ed.), *eProduction*. AUDI AG, Ingolstadt, pp. 86–126.
- Poovannan, A., 2015. Optimization of ultrasonic metal welding parameters for copper sheet to copper wire joints and numerical analysis of ultrasonic wire bonding. *Int. J. Appl. Eng. Res. (IJAER)* 10 (2), 3301–3310.
- Reisgen, U., Stein, L., 2016. Fundamentals of joining technology: welding, brazing and adhesive bonding. In: English edition, Vol. 13. DVS Media GmbH, Düsseldorf.
- Physical Principles of Ultrasonic Technology. In: Rozenberg, L.D. (Ed.), 1973. Springer-Science+Business Media, New York.
- SAE International, 2016. Performance specification for ultrasonically welded wire terminations. <https://saemobilus.sae.org/content/uscar38-1>.
- Satpathy, M.P., Moharana, B.R., Dewangan, S., Sahoo, S.K., 2015. Modeling and optimization of ultrasonic metal welding on dissimilar sheets using fuzzy based genetic algorithm approach. *Eng. Sci. Technol. Int. J.* 18 (4), 634–647.
- Sievers, N., Die elektrische Widerstandsmessung zur zerstörungsfreien Prüfung von Lötnähten am Beispiel von Hartmetall-Stahl-Verbunden. Dissertation. Technische Universität Dortmund und Vulkan-Verlag GmbH.
- Truong, C., Oudre, L., Vayatis, N., 2020. Selective review of offline change point detection methods. *Signal Process.* 167, 107299. <https://doi.org/10.1016/j.sigpro.2019.107299>.
- Völlner, G., Essers, M., 21.11.2017. Reibschweißverbinder: stoffschlüssig verbinden - optisch prüfen.
- de Vries, E., 2004. Mechanics and mechanisms of ultrasonic metal welding. The Ohio State University. Dissertation.
- Wodara, J., Adam, T., 2004. Ultraschallfügen und -trennen. Band 1 der Grundlagen der Fügetechnik. In: Fachbuchreihe Schweißtechnik, Vol. 151. DVS Verlag, Düsseldorf.
- Xing, B., Xiao, Y., Qin, Q.H., Cui, H., 2018. Quality assessment of resistance spot welding process based on dynamic resistance signal and random forest based. *Int. J. Adv. Manuf. Technol.* 94 (1–4), 327–339. <https://doi.org/10.1007/S00170-017-0889-6>.
- Zäh, M.F., Mosandl, T., Schlichenrieder, K., 2002. Ultraschall-metallschweißen. steigerung der prozesssicherheit für das ultraschall-metallschweißen. *wt Werkstatttechnik online* 92 (9), 436–440.
- Zhao, D., Ren, D., Zhao, K., Pan, S., Guo, X., 2017. Effect of welding parameters on tensile strength of ultrasonic spot welded joints of aluminum to steel – by experimentation and artificial neural network. *J. Manuf. Process.* 30, 63–74. <https://doi.org/10.1016/j.jmapro.2017.08.009>.
- Zhao, J., Li, H., Choi, H., Ma, C., Cai, W., Abell, J.A., Li, X., 2017. Transient temperature and heat flux measurement using thin-film microsensors. In: Cai, W.W. (Ed.), *Ultrasonic Welding of Lithium-Ion Batteries*. ASME Press, New York.



Florian Müller studied aerospace engineering at RWTH Aachen University. Already during his studies he dealt with various joining technology issues, including bachelor's and master's theses for applications in aerospace and electromobility. Since 2018, he has been a research assistant in the field of low-heat joining processes at the Institute of Welding and Joining Technology (ISF), and a certified International Welding Engineer since 2019. At ISF, he supervises various research projects, some industry-related, some basic research-oriented, and his work focuses on metal ultrasonic welding.



Christian Mirz, studied development and design at RWTH Aachen University. Since 2017, he is a research assistant in the field of machine dynamics at the Institute of Mechanism Design Machine Dynamics and Robotics (IGMR). At the IGMR, he supervises various research projects, some of which are industry-related and some of which are basic research-oriented. The focus of his work is the modeling of dynamic systems and vibration analysis.



Sascha Weil, studied aeronautical engineering and astronautics at RWTH Aachen University. He is a former research assistant in the field of machine dynamics at the Institute of Mechanism Design Machine Dynamics and Robotics (IGMR). The focus of his work is machine learning based classification.



Dr.-Ing. Alexander Schiebahn studied mechanical engineering with a focus on production engineering at the RWTH Aachen University until 2009. From 2009 to 2013, he worked as a research assistant in the department for resistance welding processes at the Institute of Welding and Joining Technology (ISF) at RWTH Aachen University. Mr Schiebahn also completed his training as a certified International Welding Engineer in 2009. Since August 2013, Mr Schiebahn has held the position of senior engineer for the areas of resistance welding, ultrasonic welding, friction stir welding, adhesive bonding technology and mechanical joining at ISF.



After completing his studies in mechanical engineering, Mr. Corves was awarded a doctorate in engineering from RWTH Aachen University in 1989. After industrial activities in custom mechanical engineering in Germany and Switzerland, he was appointed university professor and director of the Institute of Mechanism Design, Machine Dynamics and Robotics at RWTH Aachen University in 2000. He is chairman of the VDI advisory board "Machine Elements and Mechanism Design" and member of the scientific advisory board of the VDI-GPP. He is also chairman of IFToMM Germany.



Professor Dr.-Ing. Uwe Reisgen studied mechanical engineering at RWTH Aachen University and graduated in 1990 with a degree in engineering. He then worked as a research assistant at the Institute of Welding Technology (now ISF) at RWTH Aachen University, where he received his doctorate in 1995. As a senior engineer, Mr. Reisgen was employed at the institute from 1995-2000, and since 2000 he chaired the Joining and Testing Technology Department at Forschungszentrum Jülich. In 2007, he was appointed university professor at the Institute of Welding and Joining Technology (ISF) at RWTH Aachen University and head of the institute of the same name.